Available online at www.sciencedirect.com
ScienceDirect
Journal of Power Sources 158 (2006) 1348–1357
JOURNAL OF POWER SOURCES
www.elsevier.com/locate/jpowsour

Hydrogen production from steam and autothermal reforming of LPG over high surface area ceria

N. Laosiripojana [a,*], S. Assabumrungrat [b]

[a] *The Joint Graduate School of Energy and Environment, King Mongkut's University of Technology Thonburi, Bangkok 10140, Thailand*
[b] *Center of Excellence in Catalysis and Catalytic Reaction Engineering, Department of Chemical Engineering, Faculty of Engineering, Chulalongkorn University, Bangkok 10330, Thailand*

Received 22 September 2005; received in revised form 18 October 2005; accepted 18 October 2005
Available online 28 November 2005

Abstract

Steam and autothermal reforming reactions of LPG (propane/butane) over high surface area CeO_2 (CeO_2 (HSA)) synthesized by a surfactant-assisted approach were studied under solid oxide fuel cell (SOFC) operating conditions. The catalyst provides significantly higher reforming reactivity and excellent resistance toward carbon deposition compared to the conventional Ni/Al_2O_3. These benefits of CeO_2 are due to the redox property of this material. During the reforming process, the gas–solid reactions between the hydrocarbons present in the system (i.e. C_4H_{10}, C_3H_8, C_2H_6, C_2H_4, and CH_4) and the lattice oxygen ($O_O{}^x$) take place on the ceria surface. The reactions of these adsorbed surface hydrocarbons with the lattice oxygen ($C_nH_m + O_O{}^x \rightarrow nCO + m/2(H_2) + V_O{}^{\bullet\bullet} + 2e'$) can produce synthesis gas (CO and H_2) and also prevent the formation of carbon species from hydrocarbons decomposition reactions ($C_nH_m \Leftrightarrow nC + 2mH_2$). Afterwards, the lattice oxygen ($O_O{}^x$) can be regenerated by reaction with the steam present in the system ($H_2O + V_O{}^{\bullet\bullet} + 2e' \Leftrightarrow O_O{}^x + H_2$). It should be noted that $V_O{}^{\bullet\bullet}$ denotes as an oxygen vacancy with an effective charge 2^+.

At 900 °C, the main products from steam reforming over CeO_2 (HSA) were H_2, CO, CO_2, and CH_4 with a small amount of C_2H_4. The addition of oxygen in autothermal reforming was found to reduce the degree of carbon deposition and improve product selectivities by completely eliminating C_2H_4 formation. The major consideration in the autothermal reforming operation is the O_2/LPG (O/C molar ratio) ratio, as the presence of a too high oxygen concentration could oxidize the hydrogen and carbon monoxide produced from the steam reforming. A suitable O/C molar ratio for autothermal reforming of CeO_2 (HSA) was 0.6.

Keywords: LPG; Steam reforming; Autothermal reforming; Ceria; Solid oxide fuel cell

1. Introduction

A fuel cell is an energy conversion device that produces electrical energy with greater conversion efficiency and lower pollutant emissions than combustion processes. Among the various types of fuel cells, the solid oxide fuel cell (SOFC) has attracted considerable interest as it offers the widest range of applications, flexibility in the choice of fuel, and high system efficiency. The waste heat for SOFC can also be utilized in co-generation applications and bottoming cycles to improve the overall system efficiency. Moreover, unlike low-temperature fuel cells, the SOFC anode is not affected by carbon monoxide poisoning. Although, hydrogen is the major fuel for a SOFC, the use of other fuels such as methane, methanol, ethanol, liquefied petroleum gas (LPG), gasoline and other oil derivatives are also possible via internal or in-stack reforming. Since an SOFC is operated at such a high temperature, these hydrocarbons can be internally reformed producing a H_2/CO rich gas, which is eventually used to generate the electrical energy and heat. This operation, called indirect internal reforming (IIR-SOFC), is expected to simplify the overall SOFC system design [1].

Among the above hydrocarbon fuels, liquefied petroleum gas (LPG) is a commercial gas that is easily transported and stored on-site. This gas was proposed to be an attractive fuel for SOFC systems in remote areas where pipeline natural gas is not available [2]. LPG can also be used for auxiliary power units (APU) based on SOFC systems. Typically, the main components of

* Corresponding author. Tel.: +66 2 8729014; fax: +66 2 8726736.
E-mail address: navadol_l@jgsee.kmutt.ac.th (N. Laosiripojana).

0378-7753/$ – see front matter © 2005 Elsevier B.V. All rights reserved.
doi:10.1016/j.jpowsour.2005.10.058

LPG are propane and butane. According to the Australian LPG Association, the composition of LPG in Australia ranges from pure propane to a 40:60 mixture of propane and butane [2]. The steam reforming process has widely been used to produce hydrogen from LPG. The main products from the steam reforming of LPG are hydrogen, carbon monoxide, and carbon dioxide, however, the formation of ethane, ethylene, and methane are usually observed due to the decomposition of LPG and methanation reactions. The major difficulty in reforming LPG is the degradation of the reforming catalyst due to the possible carbon deposition from the decomposition of hydrocarbons, particularly at high temperature. Previously, steam reforming of LPG has been studied by a few researchers [2–8], and most of them have investigated the reforming of LPG over noble metal catalysts (e.g. Rh, Ru, and Pt) on oxide supports. Recupero et al. [8] reported that Pt/CeO_2 provides high reforming reactivity with low carbon formation. Suzuki et al. [3] found that Ru/CeO_2-Al_2O_3 can reform LPG with a low inlet steam requirement at 450 °C. Adding oxygen together with LPG and steam as an autothermal reforming process was reported to provide great benefits in terms of catalyst stability and low coke formation [4,5], however, the yield of hydrogen production could be reduced due to the oxidation of hydrogen by oxygen added. The attractive benefit of this operation is that the exothermic heat from the partial oxidation can directly supply the energy required for the endothermic steam reforming reaction, and so it is considered to be thermally self-sustaining process.

This work is aimed at the development of a catalyst for steam and autothermal reforming of LPG, which provides high stability and activity at a high temperature (700–900 °C) for later application in an IIR-SOFC. Although the precious metals such as Pt, Rh and Ru have been reported by several researchers to provide high activity for the reforming reactions and excellent resistant to carbon formation [9,10], the current prices of these metals are too high for commercial usage, and the availability of some precious metals such as ruthenium was too low to have a major impact on the total reforming catalyst market [11]. In view of these economical considerations, an alternative catalyst was developed and studied instead. Cerium oxide or ceria has been reported to be a catalyst in a wide variety of reactions involving oxidation or partial oxidation of hydrocarbons (e.g. automotive catalysis). A high oxygen mobility (redox property) [12], high oxygen storage capacity [13–18], strong interaction with the supported metal (strong metal–support interaction) [19] and a modifiable capability [20] render this material very interesting for catalysis. It has widely been reported, regarding the above properties, that ceria can promote the action of various metals in the reactions in which hydrogen is involved as a reactant or product [21–25]. According to the catalytic steam reforming reaction, ceria-based materials have been reported by several researchers to be promising supports among α-Al_2O_3 [26], γ-Al_2O_3 and γ-Al_2O_3 with alkali metal oxide and rare earth metal oxide [27], and $CaAl_2O_4$ [26–29]. One of the most promising ceria-based supports for the reforming reactions appeared to be Ce-ZrO_2, where the metal can be Ni, Pt or Pd [30–39]. Recently, a high resistance toward carbon deposition over ceria has been observed [40].

Importantly, CeO_2 has been reported to have reactivity toward methane decomposition at a high temperature (800–1000 °C) [41,42]. It was demonstrated that the gas–solid reaction between CeO_2 and CH_4 produces H_2 and CO, according to Eq. (1). Moreover, the reactions of the reduced ceria (CeO_{2-n}) with carbon dioxide and steam produce more CO and H_2 and regenerate the CeO_2 surface, Eqs. (2) and (3) [43–45]:

$$CH_4 + O_O{}^x = 2H_2 + CO + V_O{}^{\bullet\bullet} + 2e' \quad (1)$$

$$V_O{}^{\bullet\bullet} + 2e' + CO_2 = O_O{}^x + CO \quad (2)$$

$$V_O{}^{\bullet\bullet} + 2e' + H_2O = O_O{}^x + H_2 \quad (3)$$

$V_O{}^{\bullet\bullet}$ denotes an oxygen vacancy with an effective charge 2^+, $O_O{}^x$ is lattice oxygen, e′ is an electron which can either be more or less localized on a cerium ion or delocalized in a conduction band [46].

The major limitation for CeO_2 in high temperature applications is its low specific surface area due to the significant size reduction on thermal sintering [42] and, consequently, the reforming reactivity over CeO_2 was much lower than the conventional metallic catalysts [42]. It was reported that the methane conversion from CeO_2 after exposure in methane steam reforming conditions at 900 °C for 10 h was less than 10%. In addition, the corresponding post-reaction specific surface area for this material after exposure in methane steam reforming conditions was 1.9 $m^2\,g^{-1}$, and the observed size reduction percentage was 23% [42]. Therefore, the use of high surface area ceria (CeO_2 (HSA)) would be a good procedure to improve its catalytic performance at high operating temperatures. Several methods have recently been described for the preparation of a CeO_2 (HSA) solid solution. Among these methods, the surfactant-assisted approach was employed to prepare high surface area CeO_2 with improved textural, structural, and chemical properties [47]. Our previous publication [48] reported the achievement of CeO_2 with a high surface area and good stability after thermal treatment by this preparation method. Regarding the surfactant-assisted method, CeO_2 (HSA) is prepared by reacting a cationic surfactant with a hydrous oxide produced by co-precipitation under basic conditions. At a high pH value, conducting the precipitation of hydrous oxide in the presence of a cationic surfactant allows the cation exchange process between H^+ and the surfactant, resulting in a developed pore structure with an increase in surface area [47]. The achievement of high thermal stability for CeO_2 (HSA) is due to the incorporation of surfactants during preparation, which can reduce the interfacial energy and eventually decrease the surface tension of water contained in the pores. This could reduce the shrinkage and collapse of the catalyst during heating, which consequently helps the catalyst maintain a high surface area after calcination [47].

In the present work, the stability and activity toward steam reforming of LPG over high surface area CeO_2 (CeO_2 (HSA)) was studied and compared to those over the conventional low surface area CeO_2 (CeO_2 (LSA)), and also conventional Ni/Al_2O_3. The resistance towards carbon formation and the influence of the inlet H_2O/LPG molar ratio and temperature on product selectivities over these catalysts were determined. In

Table 1
Specific surface area of CeO_2 (HSA and LSA) after drying and calcinations at different temperatures

Catalyst	BET surface area ($m^2\ g^{-1}$) after drying or calcination at						
	100 °C	200 °C	400 °C	600 °C	800 °C	900 °C	1000 °C
CeO_2 (LSA)[a]	55	49	36	21	15	11	8.5
CeO_2 (HSA)[b]	105	97	69	48	35	29	24

[a] Conventional low surface area CeO_2 prepared by the precipitation method.
[b] Nanocomposite high surface area CeO_2 prepared by the surfactant-assisted approach.

addition, autothermal reforming of LPG was also investigated by adding oxygen at the inlet feed. The improvement in the resistance to carbon deposition by the presence of oxygen and a suitable inlet O_2/LPG molar ratio were determined. It should be noted that the contents of desulpherized LPG used in this work are 60% C_3H_8 and 40% C_4H_{10} (based on the compositions of LPG from PTT Company (Thailand)).

2. Experimental

2.1. Catalyst preparation and characterization

Conventional CeO_2 (CeO_2 (LSA)) was prepared by the precipitation of cerium chloride ($CeCl_3{\cdot}7H_2O$) from Aldrich. The starting solution was prepared by mixing 0.1 M of this metal salt solution with 0.4 M of ammonia in a 2:1 volumetric ratio. This solution was stirred by magnetic stirring (100 rpm) for 3 h, then sealed and placed in a thermostatic bath maintained at 90 °C for 3 days. The precipitate was filtered and washed with deionised water and acetone to remove the free surfactant. It was dried overnight in an oven at 110 °C, and then calcined in air at 1000 °C for 6 h.

High surface area CeO_2 (CeO_2 (HSA)) was prepared by adding an aqueous solution of the appropriate cationic surfactant, 0.1 M cetyltrimethylammonium bromide solution from Aldrich, to a 0.1 M cerium chloride. The molar ratio of ([Ce])/[cetyltrimethylammonium bromide] was kept constant at 0.8. The mixture was stirred and then aqueous ammonia was slowly added with vigorous stirring until the pH was 11.5 [47]. The mixture was continually stirred for 3 h, then sealed and placed in the thermostatic bath maintained at 90 °C for 3 days. After that, the mixture was cooled and the resulting precipitate was filtered and washed repeatedly with water and acetone. The filtered powder was then treated under the same procedures as CeO_2 (LSA). BET measurements of CeO_2 (both LSA and HSA) were carried out at different calcination temperatures in order to determine the loss of specific surface area due to the thermal sintering. As presented in Table 1, after drying, surface areas of 82 and 55 $m^2\ g^{-1}$ were observed for CeO_2 (HSA) and conventional CeO_2, respectively, and as expected, the surface area dramatically decreased at high calcination temperatures. However, the value for CeO_2 (HSA) is still appreciable after calcination at 1000 °C and it is almost three times that of the conventional CeO_2.

The redox properties and redox reversibilities of these synthesized CeO_2 (both LSA and HSA) were then determined by the temperature-programmed reduction (TPR) and temperature-programmed oxidation (TPO). TPR and TPO experiments were conducted in the presence of 5% H_2/Ar and 5% O_2/He, respectively, while the temperature of the system increased from room temperature to 900 °C for both experiments.

For comparison, Ni/Al_2O_3 (5 wt.% Ni) was also prepared by impregnating α-Al_2O_3 (from Aldrich) with $NiCl_3$. After stirring, the solution was dried and calcined at 1000 °C for 6 h. The catalysts were also reduced with 10%H_2/Ar at 500 °C for 6 h before use. After reduction, the catalysts were characterized by several physicochemical methods. The weight content of Ni in Ni/Al_2O_3 was determined by X-ray fluorescence (XRF) analysis. The reducibility and dispersion percentages of nickel were measured from temperature-programmed reduction (TPR) with 5% H_2 in helium and temperature-programmed desorption (TPD), respectively. The catalyst specific surface areas were obtained from BET measurement. All physicochemical properties of the synthesized Ni/Al_2O_3 are presented in Table 2.

2.2. Apparatus and procedures

An experimental reactor system was constructed as shown in Fig. 1. The feed gases including the components of interest (e.g. LPG, steam from the evaporator, and oxygen) and the carrier gas (helium) were introduced to the reaction section, in which a 10 mm diameter quartz reactor was mounted vertically inside a furnace. The reactivities of the catalyst toward steam reforming of LPG were determined by loading the catalyst in this quartz reactor, which was packed with a small amount of quartz wool to prevent the catalyst from moving. The inlet LPG concentration was kept constant at 5 kPa (C_3H_8/C_4H_{10} ratio of 0.6/0.4), while the inlet steam concentrations were varied depending on the inlet H_2O/LPG molar ratio requirement for each experiment (3.0, 4.0, 5.0, 6.0, and 7.0). Regarding the results in our previous publications [48], to avoid any limitations by intraparticle diffusion, the weight of catalyst was always kept constant at 50 mg, while the total gas flow was 100 $cm^3\ min^{-1}$ with a constant residence time of 5×10^{-4} g min cm^{-3} in all experiments. A Type-K

Table 2
Physicochemical properties of synthesized Ni/Al_2O_3 after reduction

Catalyst	Ni-load[a] (wt.%)	BET surface area ($m^2\ g^{-1}$)	Ni-reducibility[b] (Ni%)	Ni-dispersion[c] (Ni%)
Ni/Al_2O_3	4.9	40	92.1	4.87

[a] Measured from X-ray fluorescence analysis.
[b] Measured from temperature-programmed reduction (TPR) with 5% hydrogen.
[c] Measured from temperature-programmed desorption (TPD) of hydrogen after TPR measurement.

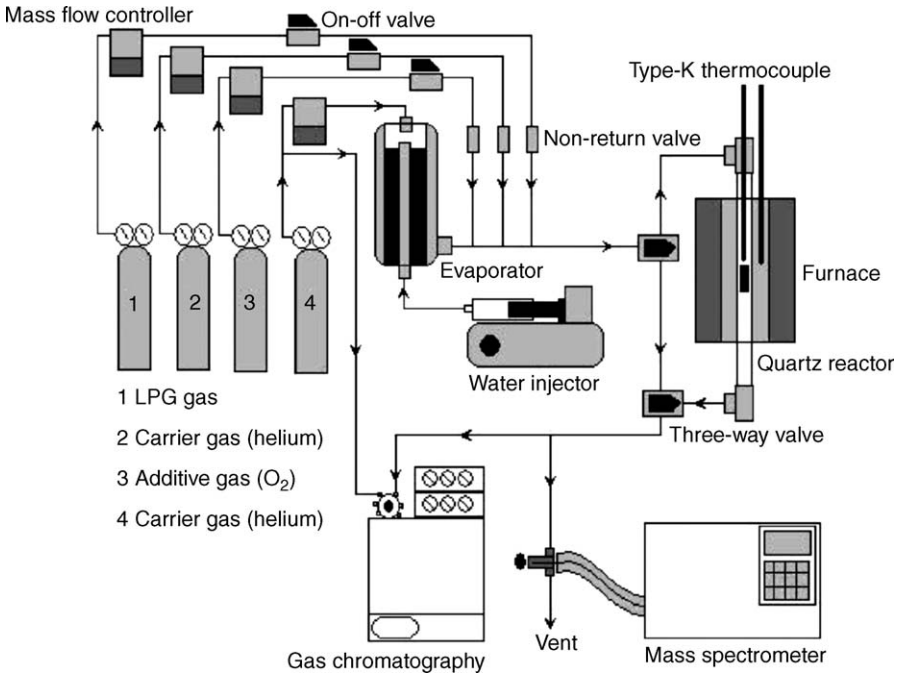

Fig. 1. Schematic diagram of the experimental set-up.

thermocouple was placed in the annular space between the reactor and the furnace. This thermocouple was mounted on the tubular reactor in close contact with the catalyst bed to minimize the temperature difference between the catalyst bed and the thermocouple. Another Type-K thermocouple was inserted in the middle of the quartz tube in order to re-check the possible temperature gradient, especially when O_2 was added along with LPG and H_2O in autothermal reforming. The recorded values showed that the maximum temperature fluctuation during the reaction was always $\pm 0.75\,^{\circ}C$ or less from the temperature specified for the reaction.

After the reactions, the exit gas mixture was transferred via trace-heated lines to the analysis section, which consisted of a Porapak Q column Shimadzu 14B gas chromatograph (GC) and a mass spectrometer (MS). Gas chromatography was used in order to investigate the steady state condition experiments, whereas the mass spectrometer, in which the sampling of the exit gas was done by a quartz capillary and differential pumping, was used in the transient carbon formation experiment. In order to study the formation of carbon species on catalyst surface, temperature-programmed oxidation (TPO) was applied by introducing 5% oxygen in helium into the system, after being purged with helium. The operating temperature was increased from room temperature to 900 °C at a rate of $10\,^{\circ}C\,min^{-1}$. The calibration of CO and CO_2 were performed by injecting a known amount of the gases from a sample loop into an injection valve in the bypass line. The response factors were obtained by dividing the number of moles for each component over the respective areas under peaks. The amount of carbon formed on the surface of catalysts was determined by measuring the CO and CO_2 yields from the TPO results (using Microcal Origin Software) assuming a value of $0.026\,nm^2$ for the area occupied by a carbon atom in a surface monolayer of the basal plane in graphite [49]. In addition to the TPO method, the amount of carbon deposition was confirmed by the calculation of carbon balance in the system. The amount of carbon deposited on the surface of catalyst would theoretically be equal to the difference between the inlet carbon containing components (C_3H_8 and C_4H_{10}) and the outlet carbon containing components (CO, CO_2, CH_4, C_2H_6, and C_2H_4). The amount of carbon deposited per gram of catalyst is given by the following equation:

$$C_{\text{deposition}} = \frac{\text{mole}_{\text{carbon(in)}} - \text{mole}_{\text{carbon(out)}}}{m_{\text{catalyst}}} \tag{4}$$

The steam reforming reactivity was defined in terms of the conversions and selectivities. Hydrocarbon conversions (propane and butane) denoted as $X_{\text{hydrocarbon}}$, and the products selectivity (hydrogen, carbon monoxide, carbon dioxide, methane, and ethylene), denoted as S_{product}, are calculated according to Eqs. (5)–(12):

$$X_{\text{butane}} = \frac{100(\%\text{butane}_{\text{in}} - \%\text{butane}_{\text{out}})}{\%\text{butane}_{\text{in}}} \tag{5}$$

$$X_{\text{propane}} = \frac{100(\%\text{propane}_{\text{in}} - \%\text{propane}_{\text{out}})}{\%\text{propane}_{\text{in}}} \tag{6}$$

$$S_{H_2} = \frac{100(\%H_2)}{3(\%\text{butane}_{\text{in}} - \%\text{butane}_{\text{out}}) + 4(\%\text{propane}_{\text{in}} - \%\text{propane}_{\text{out}}) + (\%H_2O_{\text{in}} - \%H_2O_{\text{out}})} \tag{7}$$

$$S_{CO} = \frac{100(\%CO)}{2(\%\text{butane}_{\text{in}} - \%\text{butane}_{\text{out}}) + 3(\%\text{propane}_{\text{in}} - \%\text{propane}_{\text{out}})} \tag{8}$$

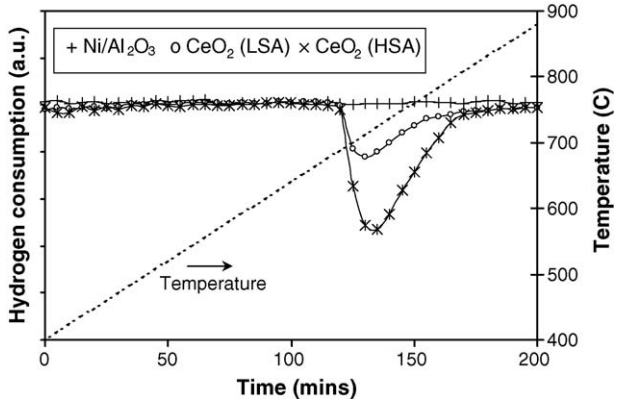

Fig. 2. Temperature-programmed reduction (TPR-1) of fresh catalysts after reduction.

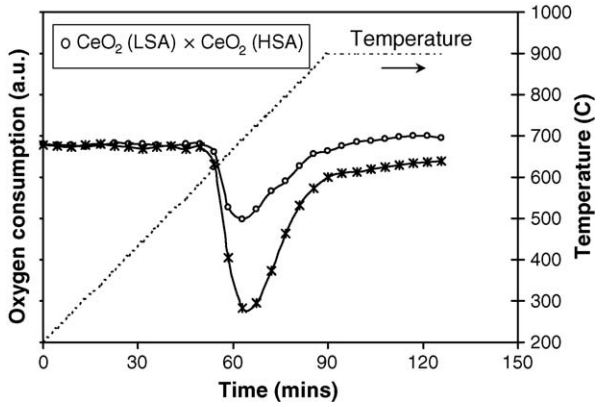

Fig. 3. Temperature-programmed oxidation (TPO) of CeO_2 (HSA and LSA) after TPR-1.

$$S_{CO_2} = \frac{100(\%CO_2)}{2(\%\text{butane}_{in} - \%\text{butane}_{out}) + 3(\%\text{propane}_{in} - \%\text{propane}_{out})} \quad (9)$$

$$S_{CH_4} = \frac{100(\%CH_4)}{2(\%\text{butane}_{in} - \%\text{butane}_{out}) + 3(\%\text{propane}_{in} - \%\text{propane}_{out})} \quad (10)$$

$$S_{C_2H_6} = \frac{100(\%C_2H_6)}{(\%\text{butane}_{in} - \%\text{butane}_{out}) + 1.5(\%\text{propane}_{in} - \%\text{propane}_{out})} \quad (11)$$

$$S_{C_2H_4} = \frac{100(\%C_2H_4)}{(\%\text{butane}_{in} - \%\text{butane}_{out}) + 1.5(\%\text{propane}_{in} - \%\text{propane}_{out})} \quad (12)$$

3. Results

3.1. Redox property and redox reversibility of the synthesized CeO_2

The oxygen storage capacities (OSC) and the redox properties of CeO_2 (both LSA and HSA) were investigated using temperature-programmed reduction (TPR-1) which was performed by heating the reduced catalysts up to 900 °C in 5%H_2 in argon. A test over Ni/Al_2O_3 was also performed for comparison. As shown in Fig. 2, hydrogen uptake was detected from both types of CeO_2 at the temperature above 650 °C. The amount of hydrogen uptake over CeO_2 (HSA) is significantly higher than that over CeO_2 (LSA), suggesting that the OSC and the redox properties strongly depend on the specific surface area of CeO_2. In contrast, no hydrogen consumption was observed from the TPR over Ni/Al_2O_3, indicating the absence of redox properties for this catalyst. The benefit of having a redox property in the reforming of LPG will be presented in Section 4. After being purged with helium, the redox reversibility for each type of CeO_2 was then determined by conducting temperature-programmed oxidation (TPO) following by a second temperature-programmed reduction (TPR-2). The TPO was carried out by heating the catalyst up to 900 °C in 5%O_2 in helium; the amount of oxygen chemisorbed was then measured, as shown in Fig. 3 and Table 3. Regarding the TPR-2 results as shown in Fig. 4 and Table 3, the amount of hydrogen uptake for CeO_2 (both LSA and HSA) were approximately similar to those from TPR-1, indicating the redox reversibility of these synthesized versions of CeO_2.

3.2. Homogenous (non-catalytic) reactions

Before studying the catalyst performance, homogeneous (non-catalytic) steam reforming of LPG was investigated. A

Table 3
Results of TPR(1), TPO, TPR(2) analyses of CeO_2 (both HSA and LSA)

Catalyst	Total H_2 uptake from TPR(1)[a] (μmol g_{cat}^{-1})	Total O_2 uptake from TPO[b] (μmol g_{cat}^{-1})	Total H_2 uptake from TPR(2)[c] (μmol g_{cat}^{-1})
CeO_2 (HSA)	2159	1044	2155
CeO_2 (LSA)	1784	867	1781

[a] Temperature-programmed reduction of the reduced catalysts (relative standard deviation = ±3%).
[b] Temperature-programmed oxidation after TPR(1) (relative standard deviation = ±1%).
[c] Re-temperature-programmed reduction after TPO (relative standard deviation = ±2%).

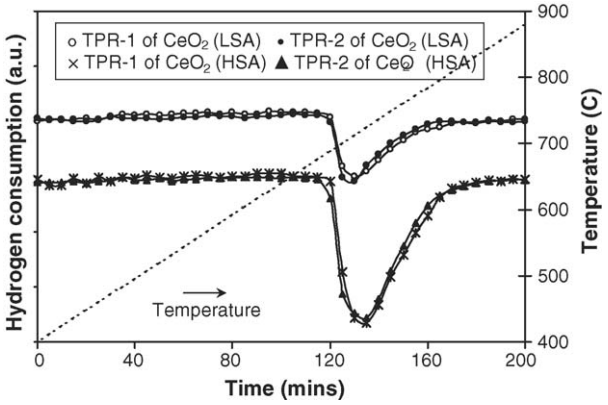

Fig. 4. Second time temperature-programmed reduction (TPR-2) of CeO_2 (HSA and LSA) compared to that of TPR-1.

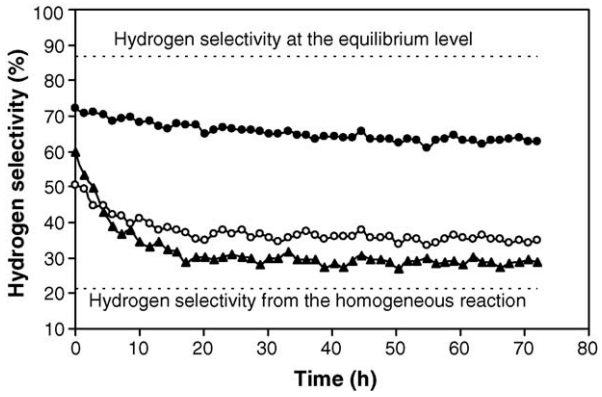

Fig. 6. Hydrogen selectivity from the steam reforming of LPG over CeO_2 (HSA) (●), CeO_2 (LSA) (◯), and Ni/Al_2O_3 (▲) at 900 °C compared to that from the homogeneous reaction and at the equilibrium level.

feed stream consisting a LPG/H_2O at a molar ratio of 1.0/5.0 was introduced into the system, while the temperature increased from ambient to 900 °C. Both propane and butane were converted to methane, ethane, ethylene, and hydrogen at the temperature above 700 °C, as shown in Fig. 5. A significant amount of carbon was also detected in the blank reactor after exposure for 10 h. These components were formed via the decomposition of butane and propane as shown in the equations below.

$$C_4H_{10} \rightarrow C_2H_6 + C_2H_4 \quad (13)$$

$$C_3H_8 \rightarrow 3/2(C_2H_4) + H_2 \quad (14)$$

$$C_2H_6 \rightarrow C_2H_4 + H_2 \quad (15)$$

$$C_2H_4 \Leftrightarrow CH_4 + C \quad (16)$$

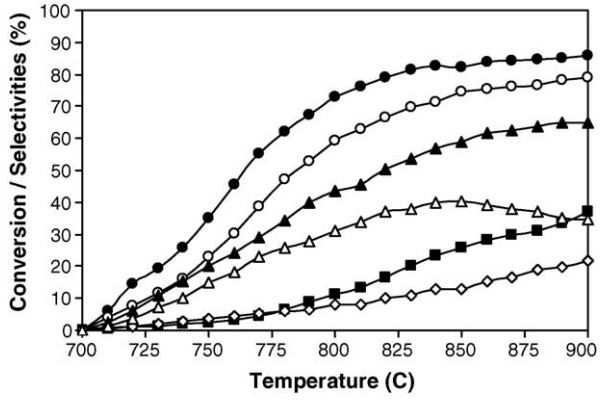

Fig. 5. Homogeneous (in the absence of a catalyst) reactivity of LPG in the presence of steam (with the inlet H_2O/LPG of 5.0) (C_4H_{10} (●), C_3H_8 (◯), C_2H_4 (▲), C_2H_6 (△), CH_4 (■), and H_2 (◊)).

There was no change in the steam concentration, and no carbon monoxide and carbon dioxide were produced in the system, indicating that the non-homogenous reforming reaction between steam and hydrocarbons did not take place at this range of conditions studied.

3.3. Stability and activity toward the steam reforming of LPG

The synthesized CeO_2 (HSA), CeO_2 (LSA), and Ni/Al_2O_3 were studied in the steam reforming of C_3H_8/C_4H_{10} at 900 °C. The feed was H_2O/LPG in helium with the molar ratio of 5.0 (H_2O/C ratio of 1.45). The reforming rate was measured as a function of time in order to determine the stability and the deactivation rate. The variations in the hydrogen selectivity with time at 900 °C are shown in Fig. 6. Significant deactivation was detected with Ni/Al_2O_3 catalyst, whereas much lower deactivations were observed for CeO_2 (HSA). Catalyst stabilities expressed as deactivation percentages are given in Table 4. It should be noted that, in order to determine whether the observed deactivation is due to the carbon formation, the post-reaction temperature-programmed oxidation (TPO) experiments were carried out.

From the TPO results shown in Fig. 7, a huge amount of carbon deposition was observed on Ni/Al_2O_3, whereas significantly less carbon formation was detected on CeO_2 (LSA) and CeO_2 (HSA) after exposure to the steam reforming conditions for 72 h. The amount of carbon formation (monolayer) on the surface of catalysts was determined by measuring the CO and CO_2 yields (using Microcal Origin Software). Using a value of 0.026 nm^2 for the area occupied by a carbon atom in a surface mono-

Table 4
Physicochemical properties of catalysts after exposure in the steam reforming of LPG at 900 °C for 72 h.

Catalyst	Deactivation (%)	C formation (monolayers)	BET surface ($m^2\ g^{-1}$)	Ni-load (wt.%)	Ni-red. (Ni%)	Ni-disp. (Ni%)
CeO_2 (HSA)	12.8	0.51[a] (0.48)[b]	22.0	–	–	–
CeO_2 (LSA)	30.6	0.92 (0.92)	7.1	–	–	–
Ni/Al_2O_3	52.3	4.73 (4.71)	~40.0	4.9	92.1	4.82

[a] Calculated using CO and CO_2 yields from temperature-programmed oxidation (TPO) with 5% oxygen.
[b] Calculated from the balance of carbon in the system.

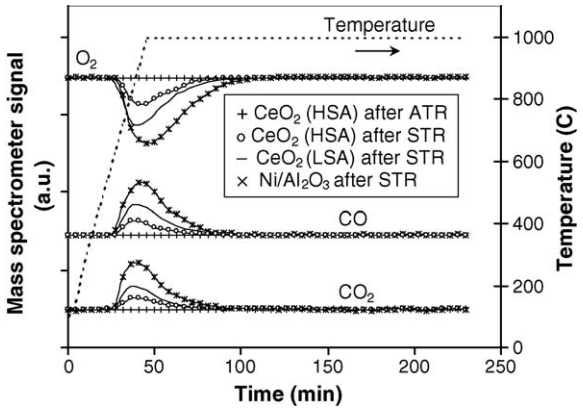

Fig. 7. Temperature-programmed oxidation (TPO) of CeO_2 (HSA), CeO_2 (LSA), and Ni/Al_2O_3 after exposure in the steam reforming (STR) and autothermal reforming (ATR) of LPG (H_2O/LPG of 5.0 for STR and O_2/LPG of 0.6 for ATR) for 72 h.

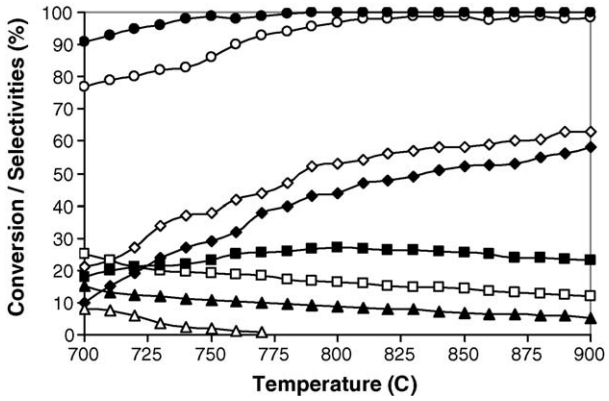

Fig. 8. Effect of reaction temperature on the conversions of C_4H_{10} (●) and C_3H_8 (○), and the selectivities of H_2 (◊), CO (♦), CO_2 (□), CH_4 (■), C_2H_6 (△), and C_2H_4 (▲) from steam reforming over CeO_2 (HSA) (with the inlet H_2O/LPG of 5.0).

layer of the basal plane in graphite [49], the quantities of carbon deposited for each catalyst were observed as in Table 4. The total amounts of carbon deposited were then verified by calculating the carbon balance of the system. Regarding the calculations, the moles of carbon deposited per gram of CeO_2 (HSA), CeO_2 (LSA), and Ni/Al_2O_3 were 0.54, 0.97, and 4.76 mmol g^{-1}. By the same assumption for the area occupied by a carbon atom [49], the values shown in Table 4 are in good agreement with the values observed from the TPO method described above. These results clearly indicate that the deactivation observed on Ni/Al_2O_3 was mainly due to carbon deposition on the surface of catalyst, and CeO_2 especially the high surface area had a significant resistance toward carbon formation as compared to Ni/Al_2O_3. BET measurements were then carried out to observe the percentage decrease in surface area of all catalysts. It should be noted that the BET measurement for Ni/Al_2O_3 was carried out after reduction of the catalyst (after TPO) with hydrogen in order to eliminate all NiO from the TRO experiment, which could affect the catalyst surface area. Results shown in Table 4 suggest that the deactivation of ceria is mainly due to the thermal sintering. However, the surface area reduction percentage of CeO_2 (HSA) is much lower than CeO_2 (LSA), indicating a higher stability toward the thermal sintering.

It should be noted that, the steady-state hydrogen selectivity observed from all catalysts (62.9% for CeO_2 (HSA), 35.0% for CeO_2 (LSA), and 28.6% for Ni/Al_2O_3) was lower than that at equilibrium state, which is approximately 87% (according to the simulation using AspenPlus 10.2), due to the incomplete decomposition of LPG to H_2, CO, and CO_2.

3.4. Effects of temperature and inlet reactants

The influences of operating temperature and the inlet steam content on the conversion of butane and propane, and the product selectivities from the steam reforming of LPG over CeO_2 (HSA) and CeO_2 (LSA) were studied by varying the operating temperature from 700 to 900 °C and changing the inlet H_2O/LPG ratio from 3.0 to 7.0 (H_2O/C ratio from 0.87 to 2.02) as represented in Figs. 8 and 9.

At 900 °C, the main products from the steam reforming reaction over CeO_2 (HSA) were CH_4, H_2 CO, and CO_2. Some formation of C_2H_4 was also observed. Hydrogen and carbon monoxide selectivities increased with increasing temperature, whereas carbon dioxide and ethylene production selectivities decreased. The dependence of methane selectivity on the operating temperature was non-monotonic, the maximum production of methane occurred at approximately 800 °C. Regarding the effect of steam, hydrogen and carbon dioxide selectivities increased with increasing inlet steam concentration, whereas carbon monoxide, methane, and ethylene selectivities decreased. These changes in product selectivities are due to the influence of the exothermic water-gas shift reaction ($CO + H_2O \rightarrow CO_2 + H_2$), whereas the decreased methane and ethylene selectivities could be due to further reforming which would generate more carbon monoxide and hydrogen. Temperature-programmed oxidations of CeO_2 (HSA) after exposure in steam reforming with different inlet H_2O/LPG ratios were then carried out to determine the effect of the inlet steam concentration on the degree of carbon formation. From the TPO results, the amount of carbon deposited slightly decreased with increasing inlet steam concentration, however, a

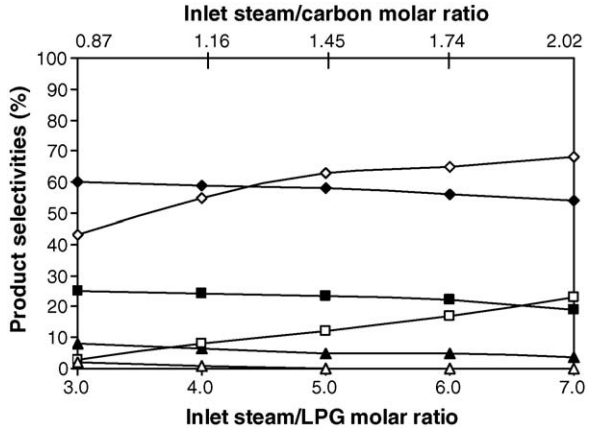

Fig. 9. Effect of inlet steam/LPG molar ratio on the selectivities of H_2 (◊), CO (♦), CO_2 (□), CH_4 (■), C_2H_6 (△), and C_2H_4 (▲) from the steam reforming of LPG over CeO_2 (HSA) at 900 °C.

Table 5
The dependence of hydrogen yield on the H_2O/LPG molar ratio and the amount of carbon formation on CeO_2 (HSA) after exposure in the steam reforming condition for 72 h

H_2O/LPG ratio	Hydrogen selectivity (%) at steady state	Total carbon formation (monolayers)
3.0	43.1	0.82[a] (0.84)[b]
4.0	55.0	0.67 (0.65)
5.0	62.9	0.51 (0.48)
6.0	65.3	0.44 (0.44)
7.0	68.0	0.41 (0.39)

[a] Calculated using CO and CO_2 yields from temperature-programmed oxidation (TPO) with 5% oxygen.
[b] Calculated from the balance of carbon in the system.

significant amount of carbon was detected even at a H_2O/LPG molar ratio of 7.0 (0.39–0.41 monolayers, Table 5).

3.5. Reactivity toward autothermal reforming

In order to reduce the degree of carbon formation and improve the product selectivities, autothermal reforming of LPG over CeO_2 (HSA) was studied by adding oxygen along with LPG and steam. The inlet H_2O/C molar ratio was kept constant at 1.45 (H_2O/LPG molar ratio of 5.0), while the inlet O/C molar ratios were varied at 0.2, 0.4, 0.6, 0.8 and 1.0. It should be noted that, while varying the ratios of H_2O/LPG and O_2/LPG, the overall space velocity was always maintained at a constant value by adjusting the flow rate of carrier gas (helium) to keep the total flow rate constant.

The effect of oxygen concentration on the product selectivities (%) at 900 °C is shown in Fig. 10. The effect of oxygen on the yields of hydrogen and carbon monoxide productions were non-monotonic. Hydrogen selectivity increased with increasing O/C molar ratio until the ratio reached 0.6. The positive effect of oxygen on the hydrogen selectivity in this range is due to the assistance of this component to reform hydrocarbons. However, higher O/C ratios showed a negative effect on the hydrogen selectivity, as too high an oxygen concentration resulted in the oxidation of the hydrogen produced from the steam reforming.

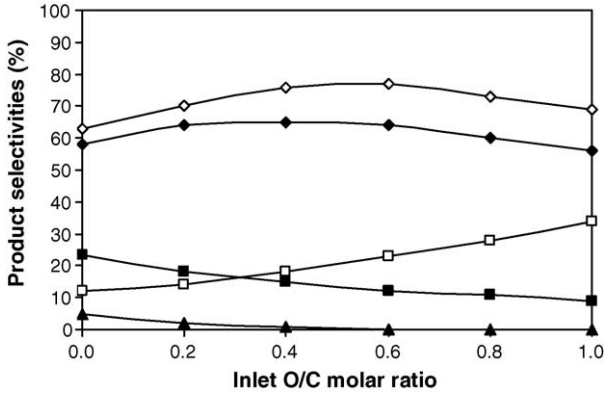

Fig. 10. Effect of inlet oxygen/carbon molar ratio on the selectivities of H_2 (◊), CO (♦), CO_2 (□), CH_4 (■), and C_2H_4 (▲) from the autothermal reforming of LPG over CeO_2 (HSA) at 900 °C.

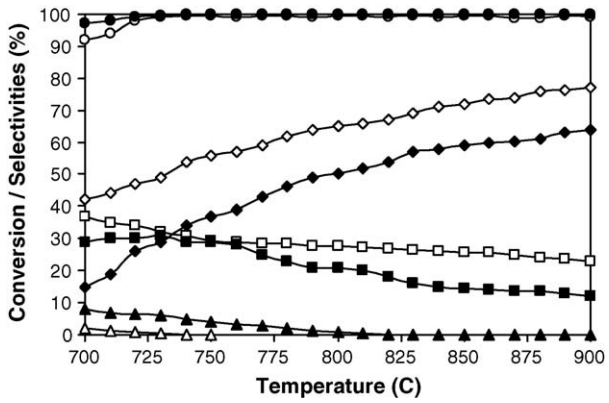

Fig. 11. Effect of reaction temperature on the conversions of C_4H_{10} (●) and C_3H_8 (●), and the selectivities of H_2 (◊), CO (♦), CO_2 (□), CH_4 (■), C_2H_6 (△), and C_2H_4 (▲) from the autothermal reforming over CeO_2 (HSA) (inlet O_2/C molar ratio of 0.6).

Table 6
The dependence of hydrogen yield on the O/C molar ratio and the amount of carbon formation on CeO_2 (HSA) after exposure in the reforming for 72 h

O/C ratio	Hydrogen selectivity (%) at steady state	Total carbon formation (monolayers)
0.0	62.9	0.51[a] (0.48)[b]
0.2	69.8	0.19 (0.21)
0.4	76.1	0.07 (0.06)
0.6	77.0	∼0.0 (∼0.0)
0.8	72.8	∼0.0 (∼0.0)
1.0	69.0	∼0.0 (∼0.0)

[a] Calculated using CO and CO_2 yields from temperature-programmed oxidation (TPO) with 5% oxygen.
[b] Calculated from the balance of carbon in the system.

Fig. 11 presents the product selectivities from the autothermal reforming of LPG (with the O/C molar ratio of 0.6) over CeO_2 (HSA) at different temperatures (700 °C to 900 °C). It was found that the main products from the autothermal reforming are similar to the steam reforming (e.g. H_2, CO, CO_2, and CH_4). Higher H_2, CO, and CO_2 selectivities were observed from autothermal reforming, whereas less CH_4, C_2H_6, and C_2H_4 were found compared to steam reforming under the same operating conditions. At 900 °C, neither C_2H_6 nor C_2H_4 formation was observed from the reaction due to the complete decomposition of these high hydrocarbons by the addition of oxygen. The benefits of the oxygen addition along with LPG and steam are presented in Section 4.

Temperature-programmed oxidation was carried out on the spent catalysts in order to determine the degree of carbon formation on the catalyst surface after exposure to the autothermal reforming reaction. From the TPO results, significantly lower quantities of deposited carbon was observed over CeO_2 (HSA) surface, and no carbon formation was detected when the inlet O/C molar ratio reached 0.6, shown in Fig. 7 and Table 6.

4. Discussion

High surface area ceria (CeO_2 (HSA)), synthesized by a surfactant-assisted approach, provided a high LPG reforming

reactivity and excellent resistance toward carbon deposition compared to conventional Ni/Al_2O_3. Carbon formation during LPG reforming could occur due to the reactions listed below:

$$C_4H_{10} \Leftrightarrow 5H_2 + 4C \quad (17)$$

$$C_3H_8 \Leftrightarrow 4H_2 + 3C \quad (18)$$

$$C_2H_4 \Leftrightarrow 2H_2 + 2C \quad (19)$$

$$CH_4 \Leftrightarrow 2H_2 + C \quad (20)$$

$$2CO \Leftrightarrow CO_2 + C \quad (21)$$

$$CO + H_2 \Leftrightarrow H_2O + C \quad (22)$$

$$CO_2 + 2H_2 \Leftrightarrow 2H_2O + C \quad (23)$$

where C is the carbonaceous deposit. At low temperature, Eqs. (22) and (23) are favorable, while Eqs. (17)–(21) are thermodynamically not favored [50]. The Boudouard reaction (Eq. (21)) and the decomposition of hydrocarbons (Eqs. (17)–(20) are the major pathways for carbon formation at such a high temperature as they show the largest change in Gibbs free energy [51]. Because of the high temperature employed in this study (700–900 °C), carbon formation via the decomposition of hydrocarbons and Boudouard reactions is possible. With the increase in steam to carbon ratio, the equilibrium of the water-gas shift reaction moves forward and produces more CO_2 rather than CO. Therefore, a high steam feed can avoid carbon deposition via the Boudouard reaction. However, a significant amount of carbon still forms due to the decomposition of hydrocarbons.

The high resistance toward carbon deposition on CeO_2, especially on high surface area CeO_2, is mainly due to the high oxygen storage capacity (OSC) of this material. CeO_2 contains a high concentration of highly mobile oxygen vacancies and thus acts as a local source or sink for oxygen on its surface. It has been reported that at high temperature, the lattice oxygen ($O_O{}^x$) at the CeO_2 surface can oxidize gaseous hydrocarbons (e.g. methane [42,48,49]). By using CeO_2 (HSA) as the catalyst, the carbon deposition due to the decomposition of hydrocarbons could be inhibited by the gas–solid reactions between the hydrocarbons present in the system (C_4H_{10}, C_3H_8, C_2H_6, C_2H_4, CH_4) and the lattice-oxygen ($O_O{}^x$) at the CeO_2 surface (Eq. (24)) forming CO_2 and H_2 from which the formation of carbon is thermodynamically unfavorable at high temperature.

$$C_nH_m + O_O{}^x \Leftrightarrow nCO + m/2H_2 + V_O{}^{\bullet\bullet} + 2e' \quad (24)$$

After the reactions, the lattice oxygen ($O_O{}^x$) is regenerated by reaction with oxygen containing compounds (e.g. steam) present in the system.

$$H_2O + V_O{}^{\bullet\bullet} + 2e' \Leftrightarrow O_O{}^x + H_2 \quad (25)$$

The redox mechanism between the hydrocarbons present in the system and the lattice oxygen ($O_O{}^x$) are illustrated below.

$$C_4H_{10} + 4S_{Ce} \Leftrightarrow 2(CH_3\text{–}S_{Ce}) + 2(CH_2\text{–}S_{Ce}) \quad (26)$$

$$C_3H_8 + 3S_{Ce} \Leftrightarrow 2(CH_3\text{–}S_{Ce}) + CH_2\text{–}S_{Ce} \quad (27)$$

$$C_2H_6 + 2S_{Ce} \Leftrightarrow 2(CH_3\text{–}S_{Ce}) \quad (28)$$

$$C_2H_4 + 2S_{Ce} \Leftrightarrow 2(CH_2\text{–}S_{Ce}) \quad (29)$$

$$CH_4 + 2S_{Ce} \Leftrightarrow CH_3\text{–}S_{Ce} + H\text{–}S_{Ce} \quad (30)$$

$$CH_3\text{–}S_{Ce} + S_{Ce} \Leftrightarrow CH_2\text{–}S_{Ce} + H\text{–}S_{Ce} \quad (31)$$

$$CH_2\text{–}S_{Ce} + S_{Ce} \Leftrightarrow CH\text{–}S_{Ce} + H\text{–}S_{Ce} \quad (32)$$

$$CH\text{–}S_{Ce} + S_{Ce} \Leftrightarrow C\text{–}S_{Ce} + H\text{–}S_{Ce} \quad (33)$$

$$C\text{–}S_{Ce} + O_O{}^x \Leftrightarrow CO + V_O{}^{\bullet\bullet} + 2e' + S_{Ce} \quad (34)$$

$$2H\text{–}S_{Ce} \Leftrightarrow H_2 + 2S_{Ce} \quad (35)$$

where S_{Ce} is the CeO_2 surface site and CH_x–S_{Ce} is an intermediate surface hydrocarbon species. S_{Ce} can be considered to be a unique site, or the same site as the lattice oxygen ($O_O{}^x$). Steele and Floyd [52] reported that the measured value of the oxygen diffusion coefficient for ceria is high and the reaction rate is controlled by a surface reaction rather than by diffusion of oxygen from the bulk of the solid particles to ceria surfaces [52]. During the reaction, hydrocarbons are adsorbed on either a unique site (S_{Ce}) or the lattice oxygen ($O_O{}^x$).

Although conventional CeO_2 (CeO_2 (LSA)) has also been reported to provide a high resistance toward carbon formation, the major drawbacks of CeO_2 (LSA) are the low specific surface area and large size reduction due to the thermal sintering, resulting in a significant drop in the redox properties compared to CeO_2 (HSA), as presented in Section 3.1, and consequently low steam reforming reactivity. The corresponding post-reaction specific surface area for CeO_2 (LSA) after exposure in reforming conditions was 7.1 $m^2\,g^{-1}$, and the observed size reduction percentage was 17%, whereas the post-reaction specific surface area for CeO_2 (HSA) was 22 $m^2\,g^{-1}$, and the observed size reduction percentage was 9%. The low redox properties of CeO_2 (LSA) also resulted in a significantly lower resistance toward carbon deposition of this material compared to CeO_2 (HSA). As described earlier, the redox reaction (Eq. (25)) between the lattice oxygen ($O_O{}^x$) at the CeO_2 surface and the hydrocarbons present in the system (C_4H_{10}, C_3H_8, C_2H_6, C_2H_4, CH_4) can prevent the formation of carbon by the decomposition of these hydrocarbon components.

It was observed from the study that the addition of oxygen along with LPG and steam in the autothermal reforming reaction reduced the degree of carbon deposition and improved the product selectivities by eliminating the formation of C_2H_6 and C_2H_4. Theoretically, oxygen prevents the formation of high hydrocarbons (i.e. C_2H_6 and C_2H_4) and subsequent carbon deposition from the decomposition reactions (Eqs. (16)–(18)) by oxidizing these hydrocarbons producing the elements that are unfavored to form carbon. The presence of oxygen also helps steam regenerate the lattice oxygen ($O_O{}^x$) on the CeO_2 surface ($O_2 + V_O{}^{\bullet\bullet} + 2e' + S_{Ce} \rightarrow O_O{}^x$). The major consideration of the autothermal reforming operation is a suitable O_2/LPG ratio. The presence of too high an oxygen concentration could oxidize the hydrogen and carbon monoxide produced from the steam reforming to steam and carbon dioxide.

5. Conclusion

High surface area ceria (CeO_2 (HSA)), synthesized in a surfactant-assisted approach, is a good catalyst for the reforming of LPG (butane and propane) at SOFC temperatures (700–900 °C) due to a high resistance towards the deactivation from carbon formation. During the reforming process, the gas–solid reactions between the hydrocarbons present in the system (i.e. propane, butane, ethane, ethylene, and methane) and the lattice oxygen (O_O^x) take place on the ceria surface, reducing the degree of carbon deposition on the catalyst surface (from hydrocarbons decomposition and Boudouard reactions). At 700–900 °C, the main products from the steam reforming of LPG over CeO_2 (HSA) were H_2, CO, CO_2, and CH_4, whereas a small amount of C_2H_4 was also observed, particularly at low temperatures. By increasing the inlet steam content, hydrogen and carbon dioxide selectivities increased, whereas carbon monoxide selectivity decreased. Moreover, the conversions of methane and ethylene were found to increase with increasing steam content in the system.

The addition of oxygen in autothermal reforming can reduce the degree of carbon deposition and eliminate the formation of higher hydrocarbons (i.e. C_2H_6 and C_2H_4). The major consideration in the autothermal reforming operation is the inlet O_2/LPG molar ratio, as the presence of too high an oxygen concentration could oxidize hydrogen and carbon monoxide, produced from the steam reforming, to steam and carbon dioxide. A suitable O/C molar ratio for autothermal reforming on CeO_2 (HSA) was observed to be 0.6.

Acknowledgement

Financial support from The Thailand Research Fund (TRF) throughout this project is gratefully acknowledged.

References

[1] P. Aguiar, D. Chadwick, L. Kershenbaum, Chem. Eng. Sci. 57 (2002) 1665.
[2] K. Ahmed, J. Gamman, K. Föger, Solid State Ion. 152–153 (2002) 485–492.
[3] T. Suzuki, H.-i. Iwanami, O. Iwamoto, T. Kitahara, Int. J. Hydrogen Energy 26 (9) (2001) 935–940.
[4] A.K. Avci, D.L. Trimm, A.E. Aksoylu, Z.I. Önsan, Catal. Lett. 88 (2003) 17–22.
[5] A.F. Ghenciu, Curr. Opin. Solid State Mater. Sci. 6 (2002) 389–399.
[6] T. Rampe, A. Heinzel, B. Vogel, J. Power Sources 86 (2000) 536–541.
[7] F. Joensen, J.R. Rostrup-Nielsen, J. Power Sources 105 (2002) 195–201.
[8] V. Recupero, L. Pino, A. Vita, F. Cipiti, M. Cordaro, M. Laganà, Int. J. Hydrogen Energy 30 (9) (2005) 963–971.
[9] L.V. Mattos, E. Rodino, D.E. Resasco, F.B. Possos, F.B. Noronha, Fuel Proc. Technol. 83 (2003) 147.
[10] H.S. Roh, K.W. Jun, S.E. Park, Appl. Catal. A 251 (2003) 275.
[11] J.R. Rostrup-Nielsen, J.-H. Bak-Hansen, J. Catal. 144 (1993) 38.
[12] P. Fornasiero, G. Balducci, R.D. Monte, J. Kaspar, V. Sergo, G. Gubitosa, A. Ferrero, M. Graziani, J. Catal. 164 (1996) 173.
[13] T. Miki, T. Ogawa, M. Haneda, N. Kakuta, A. Ueno, S. Tateishi, S. Matsuura, M. Sato, J. Phys. Chem. 94 (1990) 339.
[14] C. Padeste, N.W. Cant, D.L. Trimm, Catal. Lett. 18 (1993) 305.
[15] S. Kacimi, J. Barbier Jr., R. Taha, D. Duperz, Catal. Lett. 22 (1993) 343.
[16] G.S. Zafiris, R.J. Gorte, J. Catal. 143 (1993) 86.
[17] G.S. Zafiris, R.J. Gorte, J. Catal. 139 (1993) 561.
[18] S. Imamura, M. Shono, N. Okamoto, R. Hamada, S. Ishida, Appl. Catal. A 142 (1996) 279.
[19] L. Fan, K. Fujimoto, J. Catal. 172 (1997) 238.
[20] M. Pijolat, M. Prin, M. Soustelle, J. Chem. Soc., Faraday Trans. 91 (1995) 3941.
[21] S. Imamura, T. Higashihara, Y. Saito, H. Aritani, H. Kanai, Y. Matsumura, N. Tsuda, Catal. Today 50 (1999) 369.
[22] S. Imamura, K. Denpo, K. Utani, Y. Matsumura, H. Kanai, React. Kinet. Catal. Lett. 67 (1999) 163.
[23] S. Imamura, K. Denpo, K. Kanai, H. Yamane, Y. Saito, K. Utani, Y. Matsumura, Sekiyu Gakkaishi 44 (2001) 293.
[24] S. Imamura, H. Yamane, H. Kanai, T. Shibuta, K. Utani, K. Hamada, J. Jpn. Petrol. Inst. 45 (2002) 187.
[25] S. Imamura, Y. Taniguchi, Y. Ikeda, S. Hosokawa, H. Kanai, H. Ando, React. Kinet. Catal. Lett. 76 (2002) 201.
[26] H.S. Roh, K.W. Jun, W.S. Dong, J.S. Chang, S.E. Park, Y.I. Joe, J. Mol. Catal. A 181 (2002) 137–142.
[27] Q. Miao, G. Xiong, S. Sheng, W. Cui, L. Xu, X. Guo, Appl. Catal. A 154 (1987) 17–27.
[28] A.A. Lemonidou, M.A. Goula, I.A. Vasalos, Catal. Today 46 (1987) 175–183.
[29] W.S. Dong, H.S. Roh, K.W. Jun, S.E. Park, Y.S. Oh, Appl. Catal. A 226 (2002) 63–72.
[30] M. Mamak, N. Coombs, G. Ozin, Adv. Mater. 12 (2000) 198–202.
[31] M. Mamak, N. Coombs, G. Ozin, J. Am. Chem. Soc. 122 (2000) 8932.
[32] M. Mamak, N. Coombs, G.A. Ozin, Chem. Mater. 13 (2001) 3564.
[33] P. Bera, S. Mitra, S. Sampath, M.S. Hegde, Chem. Commun. (2001) 927.
[34] A. Martinez-Arias, J.M. Coronado, R. Cataluna, J.C. Conesa, J.C. Soria, J. Phys. Chem. B 102 (1998) 4357.
[35] D. Skarmoutsos, F. Tietz, P. Nikolopoulos, Fuel Cells 1 (2001) 243.
[36] T. Takeguchi, S.N. Furukawa, M. Inoue, J. Catal. 202 (2001) 14.
[37] J. Sfeir, P.A. Philippe, P. Moseki, N. Xanthopoulos, R. Vasquez, J.M. Hans, V.H. Jan, K.R. Thampi, J. Catal. 202 (2001) 229.
[38] N. Kiratzis, P. Holtappels, C.E. Hatchwell, M. Mogensen, J.T.S. Irvine, Fuel Cells 1 (2001) 211.
[39] H.S. Roh, W.S. Dong, K.W. Jun, S.E. Park, Chem. Lett. (2001) 88.
[40] E. Ramírez-Cabrera, A. Atkinson, D. Chadwick, Appl. Catal. B 47 (2004) 127–131.
[41] E. Ramírez-Cabrera, N. Laosiripojana, A. Atkinson, D. Chadwick, Catal. Today 78 (2003) 433–438.
[42] N. Laosiripojana, Reaction engineering of indirect internal steam reforming of methane for application in solid oxide fuel cells. Ph.D. Thesis, University of London, England, 2003.
[43] K. Otsuka, T. Ushiyama, I. Yamanaka, Chem. Lett. (1993) 1517.
[44] K. Otsuka, M. Hatano, A. Morikawa, J. Catal. 79 (1983) 493.
[45] K. Otsuka, M. Hatano, A. Morikawa, Inorg. Chim. Acta 109 (1985) 193.
[46] P.J. Gellings, J.M. Henny, Bouwmeester, Solid state aspects of oxidation catalysis, Catal. Today 58 (2000) 1–53.
[47] D. Terribile, A. Trovarelli, J. Llorca, C. de Leitenburg, G. Dolcetti, Catal. Today 43 (1998) 79–88.
[48] N. Laosiripojana, S. Assabumrungrat, Appl. Catal. B: Environ. 60 (2005) 107.
[49] E. Ramirez, A. Atkinson, D. Chadwick, Appl. Catal. B 36 (2002) 193–206.
[50] Y. Lwin, W.R.W. Daud, A.B. Mohamad, Z. Yaakob, Int. J. Hydrogen Energy 25 (1) (2000) 47–53.
[51] J.N. Amor, Appl. Catal. A 176 (1999) 159–176.
[52] B.C.H. Steele, J.M. Floyd, Proc. Br. Ceram. Soc. 19 (1971) 55.